Eurographics Workshop on Visual Computing for Biology and Medicine (2017)
I. Hotz, D. Merhof, and C. Rieder (Editors)

MRI Hip Joint Segmentation: A Locally Bhattacharyya Weighted Hybrid 3D Level Set Approach

D. D. Pham[1], C. A. Morariu[1], T. Terheiden[1], S. Landgraeber[2], M. Jäger[2], and J. Pauli[1]

[1]Intelligent Systems, Faculty of Engineering, University of Duisburg-Essen, Germany
[2]Department of Orthopaedics and Trauma Surgery, University Hospital Essen, University of Duisburg-Essen, Germany

Abstract

In this paper, we propose a novel hybrid level set approach that locally balances the combined use of both Gradient Vector Flow and region based energy cost function by means of the Bhattacharyya coefficient. The local neighborhood of each contour point is naturally divided into an area encapsulated and one excluded by the contour. We propose utilizing the Bhattacharyya coefficient of the intensity distributions of these local areas to determine a point-wise weighting scheme for the curve propagation. The performance of our method regarding segmentation quality is evaluated on the segmentation of the hip joint in 10 MRI data sets. Our proposed method shows a clear improvement compared to conventional 3D level set approaches.

CCS Concepts

•***Computing methodologies*** → *Image segmentation; Image processing;* •***Applied computing*** → *Imaging;*

1. Introduction

In modern medicine, patient-specific models of anatomical structures play an increasingly important role, as they allow simulations for various areas of tailored patient treatment. Especially the human hip joint is a structure of interest, as it carries a major portion of the body weight, therefore being naturally prone to physical deterioration. Regarding diagnosis, Cichon et al. [CRH*16] propose superimposing a simulation of the joint movement and pain registration to further investigate femoroacetabular impingement, a cause for secondary coxarthrosis that is difficult to interpret in static medical images. Tsumura et al. [TKIT05] on the other hand present a computational simulation of acetabular osteotomy for preoperative planning purposes. For these kind of patient-specific simulations, first the 3D models need to be generated by segmenting the anatomical structures of interest. Manual segmentation, however, is often a tedious and time consuming process, especially if large 3D datasets, such as MRI or CT scans are used. Additionally, expert knowledge is required to correctly label the medical data sets. Many medical segmentation approaches utilize statistical shape models (SSM) to constrain uncontrolled shape deformation in the segmentation process. Therefore, the obvious choices for hip joint segmentation would be Active Shape Models (ASM) [CT92] and Active Appearance Models (AAM) [CET98]. However, the amount of labeled medical training data is often limited, which might result in an inadequate statistical model. In this case, another likely family of segmentation methods to choose from are Active Contours, as they do not require a-priori knowledge. In contrast to Kass et al.'s original formulation of active contours as *Snakes* [KWT88], Level set methods provide a parameter free representation and were introduced by Osher and Sethian [OS88]. Major advantages of level sets are their simple and consistent formulation in higher dimensional images, and their canonical support for topological changes.
Many bone segmentation approaches utilize CT scans, as bones are more distinguishable from their background in CT scans than in MR images and therefore easier to segment. However, we choose to use MRI data sets due to the fact, that CT scans require patients to be exposed to radiation, which can be harmful, especially for young patients. This circumstance can be avoided by using MRI data sets, which are additionally more suitable to capture soft tissue components, such as the *labrum acetabulare* in case of the hip joint.

2. Related Work

2.1. Hip Joint Segmentation

Given enough labeled training data, there have already been various segmentation methods for the hip joint. Chu et al. [CCLZ15] present a fully automatic hip joint segmentation approach for CT scans, that uses random forests for landmark detection, and multi-atlantes and articulated statistical shape models for segmentation. Kainmüller et al. [KLZH09] also present a fully automatic approach for CT scans, extending the common definition of statistical shape models to *Joint Statistical Shape Models* by additionally modeling the rotational displacement of femur to pelvis. Xia

DOI: 10.2312/vcbm.20171243

et al. [XFC*13] compare multi-atlas-based methods to ASM-based approaches for hip joint segmentation from MR images. Schmid et al. [SMT08] propose a deformable model approach utilizing Principle Component Analysis of global shape variations and Markov Random Field of local deformations to segment bone structures from low resolution MRI datasets.

2.2. Related Level Set Approaches

Caselles et al. [CKS97] introduce an edge-based level set formulation, in which the contour propagates by means of energy minimization on manifolds. Chan and Vese on the other hand formulate the concept of active contours without edges as region-based level sets [CV01]. Lankton et al. [LT08] propose a point-wise localization scheme for general region-based level sets, and Jung and Jung [JJ08] suggest a trade-off solution between Lankton's localization and Chan and Vese's global formulation by only considering contour points as well as points that are within an inner and outer band of the contour. Zhang et al. [ZMSM08] also propose a hybrid level set approach, combining Caselles et al.'s edge-based approach with Chan and Vese's region-based formulation, using arbitrary weights. In contrast to Zhan et al.'s work we present a hybrid approach using Xu and Prince's Gradient Vector Flow (GVF) Field [XP98] and a semi-localized formulation of Chan and Vese's method, based on Jung and Jung's work. Additionally, we suggest a point-wise weighting, utilizing the Bhattacharyya coefficient [Bha43] within a point-wise local neighborhood, motivated by Lankton et al.'s localization scheme.

3. Method

3.1. Level Set Methods

The general idea behind the level set formulation of active contours is to represent a closed contour Γ as the intersection of the graph of a higher dimensional embedding function and the zero-level set. Let $I : \Omega \subseteq \mathbb{R}^n \rightarrow \mathbb{R}$ denote an n-dimensional image. Then the embedding function $\Phi : \Omega \rightarrow \mathbb{R}$ is defined, such that $\{p|\Phi(p) = 0\} = \Gamma$. A simple embedding function is the signed distance function, that returns the shortest distance of a given point $p \in \Omega$ to the contour Γ, differentiating between points inside, outside, and on the contour. Thus, enclosed points can easily be differentiated from excluded points and contour points by means of Φ. With this formulation, the contour deformation towards object boundaries is implicitly achieved by modifying Φ with the following general update equation:

$$\Phi^{t+1} = \Phi^t + \frac{\partial \Phi^t}{\partial t}, \tag{1}$$

where Φ^t denotes the embedding function at time t.
Edge based level set methods use prominent edges in the image as orientation for the contour evolution. In case of geodesic contours the update term

$$\frac{\partial \Phi^t}{\partial t} := \omega |\nabla \Phi^t| div\left(\frac{\nabla \Phi^t}{|\nabla \Phi^t|}\right) + \nabla \omega^T \nabla \Phi^t, \tag{2}$$

is used according to Caselles et al. [CKS97], where ω is an edge indicator function. The first term represents the scaled mean curvature motion, and the second term ensures the propagation towards edges.
However, in *region based* approaches, the contour propagation is determined by minimization of an energy function $E(\Phi^t)$, that depends on image statistics within the regions inside and outside the contour, which will be referred to as *inner* and *outer* region, respectively. In a gradient descent manner, (1) can be modified to

$$\Phi^{t+1} = \Phi^t - \nabla_{\Phi^t} E. \tag{3}$$

A common energy is the Chan-Vese energy presented by Chan and Vese [CV01]. It penalizes intensity deviations from their respective region's current mean intensity and is formalized as

$$E_{CV}(\Phi^t) := \int_\Omega \mathcal{H}(\Phi^t(p))|I(p) - \mu_{in}(\Phi^t)|^2 + \mathcal{H}(-\Phi^t(p))|I(p) - \mu_{out}(\Phi^t)|^2 \, \mathbf{d}p, \tag{4}$$

where

$$\mathcal{H}(l) := \begin{cases} 1 & , \text{if } l \geq 0 \\ 0 & , \text{else} \end{cases} \tag{5}$$

is the Heaviside function for some level $l \in \mathbb{R}$ and μ_{in} and μ_{out} denote the mean intensities of inner and outer region, respectively, given current Φ^t.

3.2. Incorporation of Gradient Vector Flow Field in Level Sets

Xu and Prince [XP98] present the Gradient Vector Flow (GVF) Field as a new external energy for Snakes to overcome the shortcomings of the traditional gradient based formulation, such as noise-sensitivity, limited impact of strong edges on contour propagation, and inability to segment concave objects. The GVF field is a vector field $\mathbf{v}^*$, that determines the evolution of each contour point. Given $\mathbf{v}^*$, the gradient vector field $\nabla\omega$ in (2) can be replaced by $\mathbf{v}^*$, resulting in the GVF field based update term

$$\frac{\partial \Phi^t}{\partial t}(p) = \omega(p)|\nabla \Phi^t(p)| div\left(\frac{\nabla \Phi^t(p)}{|\nabla \Phi^t(p)|}\right) + \mathbf{v}(p)^{*T} \nabla \Phi^t(p). \tag{6}$$

3.3. Semi-Localization of Chan Vese Energy

Chan and Vese [CV01] propose a global energy approach, where the entire inner and outer regions are considered. However, the outer area can be large and often contains many different structures, potentially providing misleading information for the contour deformation. Therefore, we suggest semi-localizing the region of interest onto a band with radius r around the current contour, which is loosely based on Jung and Jung's work [JJ08]. In contrast to Lankton's localization approach [LT08], where the energy is calculated point-wise and therefore decoupled, in our variant a global energy is nevertheless employed. However, the points contributing to the energy are restricted to a band inside and outside the current contour. Because of the need for reinitialization of Φ^t in level set methods, we get $0 < \Phi^t(p) < r$ for points in the outer band and $-r < \Phi^t(p) < 0$ for all points in the inner band. For the formal description we therefore modify the original Heaviside function to

$$\mathcal{H}_{+r}(l) = \begin{cases} 1 & , \text{if } 0 < l < r \\ 0 & , \text{else} \end{cases}$$

and $\mathcal{H}_{-r}(l)$ accordingly for arbitrary level $l \in \mathbb{R}$, to be able to access the points within the inner and outer band, respectively. The mean intensity of the outer band is denoted by $\mu_{+r}(\Phi^t)$, and $\mu_{-r}(\Phi^t)$ represents the mean intensity of the inner band. The global Chan Vese energy can then be reformulated in a semi-local fashion to

$$E_{CV_{SL}}(\Phi^t) := \int_\Omega \mathcal{H}_{-r}(\Phi^t(p))|(I(p) - \mu_{-r}(\Phi^t)|^2 + \mathcal{H}_{+r}(\Phi^t(p))|I(p) - \mu_{+r}(\Phi^t)|^2 \,\mathbf{d}p. \tag{7}$$

Using calculus of variations the negative gradient $-\nabla_{\Phi^t} E_{CV_{SL}}$ is derived as

$$\frac{\partial \Phi^t}{\partial t}(p) := -\delta_{-r}(\Phi^t(p))|I(p) - \mu_{-r}(\Phi^t)|^2 + \delta_{+r}(\Phi^t(p))|I(p) - \mu_{+r}(\Phi^t)|^2, \tag{8}$$

where δ_{-r} and δ_{+r} represent the derivatives of $\mathcal{H}_{-r}$ and $\mathcal{H}_{+r}$ for $r > 0$, respectively.

3.4. Hybrid Approach

The hybrid approach aims to combine the GVF-based level set formulation with the semi-localized Chan Vese energy, described in the previous sections. As the update terms (6) and (8) each pull the contour towards respective local energy minima, the weighted linear combination of both terms $\frac{\partial \Phi^t}{\partial t} := \alpha F_{GVF} + \beta F_{CV_{SL}}$ with $\alpha, \beta \geq 0$ and $\alpha + \beta = 1$, will pull the contour towards local minima of the linear combination of both energy functionals. F_{GVF} and $F_{CV_{SL}}$ denote the update terms (6) and (8), respectively. If the current contour is located in a rather homogeneous area, in which inner and outer band region do not significantly differ, the GVF term F_{GVF} is preferred to the semi-local term $F_{CV_{SL}}$, as F_{GVF} has a wider impact range. We propose utilizing the Bhattacharyya coefficient as weighting scheme. The Bhattacharyya coefficient Bh measures the relative similarity between two probability distributions pr_1 and pr_2 as

$$Bh(pr_1, pr_2) := \int \sqrt{pr_1(m) \cdot pr_2(m)}\mathrm{d}m$$

with the property $0 \leq Bh(pr_1, pr_2) \leq 1$.
For the hybrid method, we consider the local neighborhood of each contour point and compute the Bhattacharyya coefficient of the intensity distributions of the inner and outer regions. We choose the local neighborhood based on Lankton et al.'s localization approach. Fig. 1 illustrates the local neighborhood of a contour point from which the intensity distributions are computed. Given a radius $r > 0$ the neighboring points of interest can be extracted by the indicator function

$$\mathcal{B}_r(p,q) := \begin{cases} 1 & , \text{if } ||p-q|| < r \\ 0 & , \text{else,} \end{cases}$$

where $p \in \Gamma$ is the current contour point and $q \in \Omega$ an arbitrary point in the domain. With the help of the original Heaviside function as in Eq. (5) and the indicator function

$$\chi(m,n) := \begin{cases} 1 & , \text{if } n = m \\ 0 & , \text{else,} \end{cases}$$

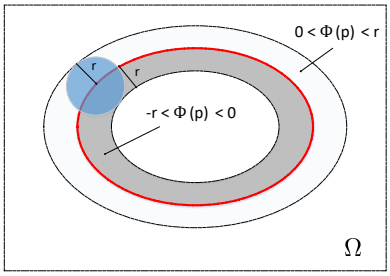

Figure 1: *Lankton-Localization for Bhattacharyya weighting*

where $m, n \in \mathcal{R}$ denote arbitrary (gray-) values that need to be compared, the intensity distributions of the inner and outer regions of the contour point $p \in \Gamma$, given a radius $r > 0$, are formalized by

$$pr_{in}(r,p,m) := \frac{\int_{q\in\Omega} \mathcal{B}_r(p,q)\mathcal{H}(-\Phi^t(q))\chi(m, I(q))\mathrm{d}q}{\int_{q\in\Omega} \mathcal{B}_r(p,q)\mathcal{H}(-\Phi^t(q))\mathrm{d}q}$$

and $pr_{out}(r,p,m)$ accordingly, where $m \in \mathbb{R}$ denotes an arbitrary gray value. Thus, if the embedding function Φ^t, the radius $r > 0$, and the contour point $p \in \Gamma$ are given, the intensity distributions $pr_{in}(r,p,m)$ and $pr_{out}(r,p,m)$ are canonically implied. Therefore, we can calculate the Bhattacharyya coefficient for each contour point $p \in \Gamma$, given the same radius $r > 0$ as the band for semi-localization by means of

$$Bh_\Gamma(r,p) := \int_{m\in I(\Omega)} \sqrt{pr_{in}(r,p,m) \cdot pr_{out}(r,p,m)}\mathrm{d}m.$$

If the intensity distributions of inner and outer region are rather similar, $Bh_\Gamma(r,p)$ reaches values close to 1. In this case, we want to weight F_{GVF} more heavily than $F_{CV_{SL}}$, as F_{GVF} has a wider impact range. Hence, we propose the point-wise weighting scheme with $\alpha(p) := Bh_\Gamma(r,p)$ and $\beta(p) := 1 - Bh_\Gamma(r,p)$ for the contour point $p \in \Gamma$ and $r > 0$. To ensure the comparability of F_{GVF} and $F_{CV_{SL}}$ a factor $\zeta := \frac{\max|F_{GVF}|}{\max|F_{CV_{SL}}|}$ is introduced to scale $F_{CV_{SL}}$ with respect to F_{GVF}. Altogether the new update term for our hybrid approach is defined as

$$\frac{\partial \Phi^t}{\partial t}(p) := \alpha(p)F_{GVF}(p) + \beta(p)\zeta F_{CV_{SL}}(p).$$

4. Experiments

We evaluated our proposed approach on 10 T1-weighted MRI datasets of 8 different patients, as two patients were examined both before and after surgical procedures. The MR images were recorded using a *Siemens Magnetom Area 1,5 Tesla* MR tomograph. The respective ground truths were validated by physicians. As the hip joint consists of a joint socket (*acetabulum*) and a joint head (*femur head*), for each data set a 3D shape model of the acetabulum and a model for the femur head is generated from the ground truths of the remaining patients as the mean of their statistical shape models. We chose this procedure to avoid biased initial shapes in our evaluation. However, any arbitrary 3D model of acetabulum and femur head are sufficient for our approach. This model is then manually positioned, rotated, and scaled within

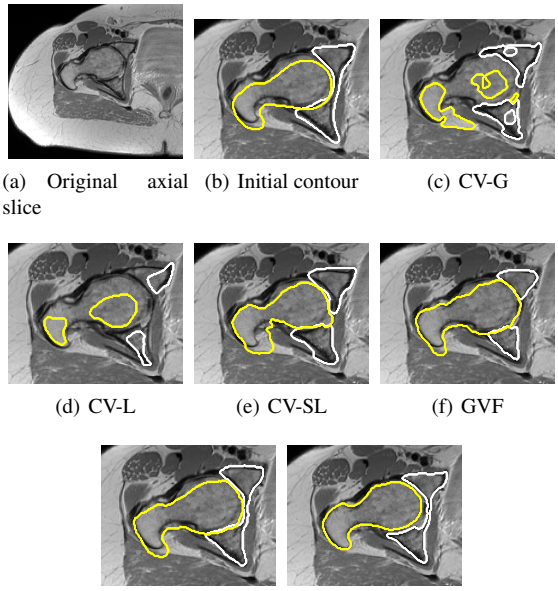

(a) Original axial slice (b) Initial contour (c) CV-G

(d) CV-L (e) CV-SL (f) GVF

(g) Hybrid (h) Ground Truth

Figure 2: *(a) Whole axial slice of exemplary data set with (b) initial contour, (c)-(g) segmentation results of each method at iteration $n = 200$, and (h) ground truth. For better visualization of the contours (b)-(h) are zoomed in. The femur head is depicted in yellow and acetabulum in white.*

	$n = 0$	$n = n^*$				
	Initial	CV-G	CV-L	CV-SL	GVF	Hybrid
FH						
∅	0.79	0.80	0.80	0.81	0.84	0.84
std	0.03	0.02	0.02	0.02	0.02	0.02
AC						
∅	0.82	0.84	0.83	0.83	0.86	0.87
std	0.02	0.02	0.02	0.02	0.01	0.01

Table 1: *DSC segmentation results for the femur head (FH) and acetabulum (AC) of each data set at initiation $n = 0$, and at iteration $n = n^*$, where the best result was achieved*

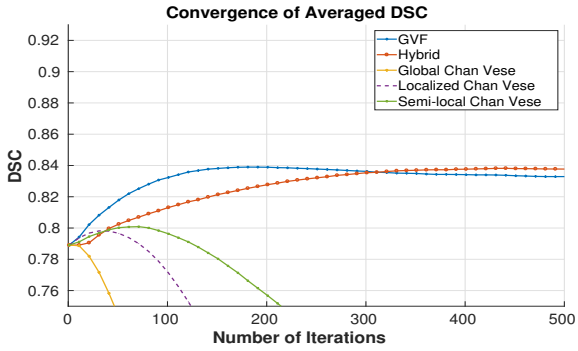

Figure 3: *DSC-Convergence of Level Set Methods (Femur head)*

the MRI data set, for acetabulum and femur head, respectively, to serve as initial contours for our level set approach. The Dice Similarity Coefficient (DSC) was used to measure segmentation quality every 10 iterations within 500 iterations for each data set. The results were compared to Lankton's 3D implementation of the global Chan Vese approach (CV-G), his localized method with the Chan Vese energy (CV-L), our proposed semi-local Chan Vese energy approach based on Jung and Jung (CV-SL), and the GVF-based method (GVF). For these methods we used grid search to establish the most promising parameter settings to compare with our approach. The CV-G and CV-L implementations were provided by Lankton [Lan07]. We used the same initial contours for each method to ensure comparability. For the local and hybrid approaches we used a radius of 9 voxels. Exemplary segmentation results of the whole hip joint are shown in Fig. 2, in which an axial slice is pictured with the corresponding 2D contour slices of the 3D segmentations.

4.1. Femur head

Table 1 shows the initial mean DSC and the mean DSC of the best segmentation results of the femur head (FH) achieved by the respective methods at iteration $n = n^* \in \{0, 10, 20, \ldots 500\}$ for each data set. n^* denotes the number of iterations for which the best DSC result was achieved. It is easy to notice that the GVF-based approach and our proposed method achieve the most promising improvements regarding mean DSC, while the Chan Vese energy based methods only show little or no improvement. This observation is also visible over time, as Fig. 3 shows the averaged DSC over all data sets plotted against the number of iterations. While the DSC values of the Chan Vese methods decrease after an initial improvement, the GVF-based approach shows the fastest increase, followed by our hybrid method. Surprisingly, CV-G and CV-L perform poorly on 3D data sets. As for CV-G, given the whole image for energy generation as in Eq. (4), the mean intensity of the outer region is heavily influenced by image regions, that are far away from the object boundary. The poor performance of CV-L is due to the fixed radius $r > 0$ for all contour points. While the radius for some contour points seem to be chosen sufficient to drive the contour towards the object boundary, as seen in the lower contour parts in Fig. 2 (d), the same radius might be too small or too large for other contour points, especially in a 3D context. Although GVF shows a faster increase in segmentation quality in time, a slight continuing decrease is visible from around $n \approx 180$ on, while our approach shows convergence (see Fig. 3).

4.2. Acetabulum

In Table 1 the initial mean DSC and the mean DSC of the best segmentation results of the acetabulum achieved by the respective methods at iteration n^* for each data set are listed. Like for the segmention of the femur head, the GVF-based approach and our proposed method show the most promising improvements, while the Chan Vese energy based methods only achieve little improvement. Taking into consideration Fig. 4, in which the convergence behavior of the averaged DSCs over all data sets from each level set method is illustrated, one can observe that initial improvements

of the Chan Vese based methods, are merely temporary, as their graphs rapidly decrease in time. Again, GVF shows the earliest improvement, however, the graph decreases shortly thereafter, and intersects the rising graph of our proposed approach. Nonetheless, the graph of our approach also slightly drops at around iteration $n \approx 300$. The worsening of GVF's and Hybrid's mean DSCs is due to the fact, that in the acetabulum, there exists a bone region, that is rather narrow. This part of the bone is difficult to segment for all approaches, as can be seen in Fig. 2, where all considered methods except for our hybrid approach fail to capture the narrow part of the hip joint. However, our hybrid approach also gradually

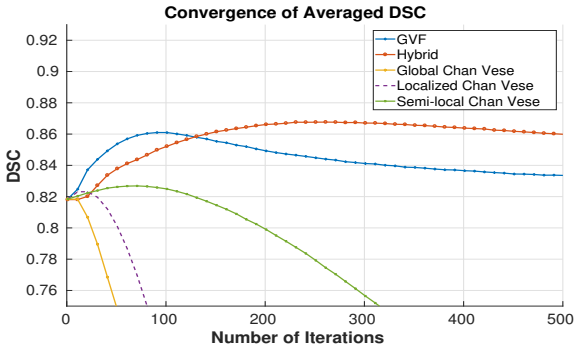

Figure 4: *DSC-Convergence of Level Set Methods (Acetabulum)*

excludes this narrow bone area, such that a slight decrease of its graph in Fig. 4 becomes noticeable. Our proposed method altogether achieves better results than GVF due to its combination with CV-SL by means of the proposed local Bhattacharyya weighting scheme.

5. Conclusion

In this paper, we propose a hybrid 3D level set method, that combines the GVF-based approach with a semi-localized variant of Chan and Vese's region-based energy formulation by means of a Bhattacharyya coefficient-based, Lankton-local weighting scheme. Our method analyses the local neighborhood of each contour point to determine if F_{GVF} or $F_{CV_{SL}}$ is more suitable for this area. Our contribution is threefold:

- We adapted Jung and Jung's approach [JJ08] to formulate the semi-localization of Chan und Vese's global energy suggestion.
- We formalized our proposed local Bhattacharyya coefficient-based weighting scheme.
- We evaluated our approach and compared it to conventional 3D level set approaches on the example of hip joint segmentation.

With our proposed method we were able to improve level set based hip joint segmentation in 3D MRI data sets compared to conventional methods. We are aiming to extend our method by an adaptive window size approach, as suggested by Hoogi et al. [HBC*17], and adaptive window orientation control. Additionally, we would like to apply our approach on anatomical structures with a higher degree of variation, such as the thyroid and other organs with soft tissue.

References

[Bha43] BHATTACHARYYA A.: On a measure of divergence between two statistical population defined by their population distributions. *Bulletin Calcutta Mathematical Society 35*, 99-109 (1943), 28. 2

[CCLZ15] CHU C., CHEN C., LIU L., ZHENG G.: FACTS: Fully automatic CT segmentation of a hip joint. *Annals of biomedical engineering 43*, 5 (2015), 1247–1259. 1

[CET98] COOTES T. F., EDWARDS G. J., TAYLOR C. J.: Active appearance models. In *European conference on computer vision* (1998), Springer, pp. 484–498. 1

[CKS97] CASELLES V., KIMMEL R., SAPIRO G.: Geodesic active contours. *International journal of computer vision 22*, 1 (1997), 61–79. 2

[CRH*16] CICHON R., RAAB D., HEWERA S., LAZIK-PALM A., THEYSOHN J., LANDGRAEBER S., KOWALCZYK W.: The investigation of femoroacetabular impingement using motion capture, FEM and multi-body simulations. *PAMM 16*, 1 (2016), 77–78. 1

[CT92] COOTES T. F., TAYLOR C. J.: Active shape models - 'smart snakes'. In *BMVC92*. Springer, 1992, pp. 266–275. 1

[CV01] CHAN T. F., VESE L. A.: Active contours without edges. *IEEE Transactions on image processing 10*, 2 (2001), 266–277. 2

[HBC*17] HOOGI A., BEAULIEU C. F., CUNHA G. M., HEBA E., SIRLIN C. B., NAPEL S., RUBIN D. L.: Adaptive local window for level set segmentation of CT and MRI liver lesions. *Medical image analysis 37* (2017), 46–55. 5

[JJ08] JUNG H.-R., JUNG M.-R.: An implicit active contour model for feature regions and lines. *Advances in Multimedia Modeling* (2008), 35–44. 2, 5

[KLZH09] KAINMUELLER D., LAMECKER H., ZACHOW S., HEGE H.-C.: An articulated statistical shape model for accurate hip joint segmentation. In *Engineering in Medicine and Biology Society, 2009. EMBC 2009. Annual International Conference of the IEEE* (2009), IEEE, pp. 6345–6351. 1

[KWT88] KASS M., WITKIN A., TERZOPOULOS D.: Snakes: Active contour models. *International journal of computer vision 1*, 4 (1988), 321–331. 1

[Lan07] Level Set Matlab Implementation by lankton. http://www.shawnlankton.com/2009/04/sfm-and-active-contours/, 2007. Accessed: 2017-01-01. 4

[LT08] LANKTON S., TANNENBAUM A.: Localizing region-based active contours. *IEEE transactions on image processing 17*, 11 (2008), 2029–2039. 2

[OS88] OSHER S., SETHIAN J. A.: Fronts propagating with curvature-dependent speed: algorithms based on Hamilton-Jacobi formulations. *Journal of computational physics 79*, 1 (1988), 12–49. 1

[SMT08] SCHMID J., MAGNENAT-THALMANN N.: Mri bone segmentation using deformable models and shape priors. In *International conference on medical image computing and computer-assisted intervention* (2008), Springer, pp. 119–126. 2

[TKIT05] TSUMURA H., KAKU N., IKEDA S., TORISU T.: A computer simulation of rotational acetabular osteotomy for dysplastic hip joint: Does the optimal transposition of the acetabular fragment exist? *Journal of Orthopaedic Science 10*, 2 (2005), 145–151. 1

[XFC*13] XIA Y., FRIPP J., CHANDRA S. S., SCHWARZ R., ENGSTROM C., CROZIER S.: Automated bone segmentation from large field of view 3D MR images of the hip joint. *Physics in medicine and biology 58*, 20 (2013), 7375. 2

[XP98] XU C., PRINCE J. L.: Snakes, shapes, and gradient vector flow. *IEEE Transactions on image processing 7*, 3 (1998), 359–369. 2

[ZMSM08] ZHANG Y., MATUSZEWSKI B. J., SHARK L.-K., MOORE C. J.: Medical image segmentation using new hybrid level-set method. In *BioMedical Visualization, 2008. MEDIVIS'08. Fifth International Conference* (2008), IEEE, pp. 71–76. 2